NeuroImage 274 (2023) 120094

Contents lists available at ScienceDirect

NeuroImage

journal homepage: www.elsevier.com/locate/neuroimage

Vessel distance mapping: A novel methodology for assessing vascular-induced cognitive resilience

Berta Garcia-Garcia[a,1,*], Hendrik Mattern[a,b,c,1], Niklas Vockert[a], Renat Yakupov[a,d], Frank Schreiber[a,e], Marco Spallazzi[f], Valentina Perosa[e,g], Aiden Haghikia[a,c,e], Oliver Speck[a,b,c,h], Emrah Düzel[a,c,d,e,i], Anne Maass[a,1], Stefanie Schreiber[a,c,e,1]

[a] German Center for Neurodegenerative Diseases, 39120 Magdeburg, Germany
[b] Biomedical Magnetic Resonance, Otto-von-Guericke-University Magdeburg, 39120 Magdeburg, Germany
[c] Center for Behavioral Brain Sciences (CBBS), 39106 Magdeburg, Germany
[d] Institute of Cognitive Neurology and Dementia Research, Otto-von-Guericke University, 39120 Magdeburg, Germany
[e] Department of Neurology, Otto-von-Guericke University, 39120, Magdeburg, Germany
[f] Department of Medicine and Surgery, Unit of Neurology, Azienda Ospedaliero-universitaria, 43126 Parma, Italy
[g] J. Philip Kistler Stroke Research Center, Massachusetts General Hospital, Boston, MA 02114, USA
[h] Leibniz Institute for Neurobiology, 39118 Magdeburg, Germany
[i] Institute of Cognitive Neuroscience, University College London, London WCIN 3AZ, UK

ARTICLE INFO

Keywords:
Vessel distance mapping
circle of Willis
Hippocampus
Cerebral small vessel disease
cognition

ABSTRACT

The association between cerebral blood supply and cognition has been widely discussed in the recent literature. One focus of this discussion has been the anatomical variability of the circle of Willis, with morphological differences being present in more than half of the general population. While previous studies have attempted to classify these differences and explore their contribution to hippocampal blood supply and cognition, results have been controversial. To disentangle these previously inconsistent findings, we introduce Vessel Distance Mapping (VDM) as a novel methodology for evaluating blood supply, which allows for obtaining vessel pattern metrics with respect to the surrounding structures, extending the previously established binary classification into a continuous spectrum. To accomplish this, we manually segmented hippocampal vessels obtained from high-resolution 7T time-of-flight MR angiographic imaging in older adults with and without cerebral small vessel disease, generating vessel distance maps by computing the distances of each voxel to its nearest vessel. Greater values of VDM-metrics, which reflected higher vessel distances, were associated with poorer cognitive outcomes in subjects affected by vascular pathology, while this relation was not observed in healthy controls. Therefore, a mixed contribution of vessel pattern and vessel density is proposed to confer cognitive resilience, consistent with previous research findings. In conclusion, VDM provides a novel platform, based on a statistically robust and quantitative method of vascular mapping, for addressing a variety of clinical research questions.

1. Introduction

The association between cerebral blood supply and cognition has gained increasing interest in recent years. Given that the brain has little to no energy reserve, a finely regulated blood supply is needed to allow the brain to meet its metabolic demands, promote local neuroplasticity (Düzel et al., 2016), and clear metabolites such as β-amyloid (Schreiber et al., 2020). Consistent observations over time have acknowledged blood supply abnormalities as a contributor to cognitive decline and dementia (Binnewijzend et al., 2016; Gorelick et al., 2017; Leeuwis et al., 2018; Fouda et al., 2019).

Although the circle of Willis is the main cranial pathway of collateral arterial circulation, in more than 50% of the population, variations of the classical closed ring-like contour are present

Abbreviations: AChA, anterior choroidal artery; ADAScog, Alzheimer's Disease Assessment Scale, cognitive subscale; aHC, anterior hippocampus; CAA, cerebral amyloid angiopathy; CSVD, cerebral small vessel disease; PCA, posterior cerebral artery; PComA, posterior communicating artery; pHC, posterior hippocampus; CoMD, center of mass distance; root-mean-squares, (RMS); ToF, time-of-flight; uB, uncal branch (AChA-independent); VDM, vessel distance mapping; VS-VDM, vessel-specific VDM; wHC, whole hippocampus.

* Corresponding author at: German Center for Neurodegenerative Diseases, Leipziger Strasse 44 (Haus 64), 39120 Magdeburg, Germany.
E-mail address: Berta.Garcia-Garcia@dzne.de (B. Garcia-Garcia).

[1] Contributed equally to the work.

https://doi.org/10.1016/j.neuroimage.2023.120094.
Received 14 April 2022; Received in revised form 30 March 2023; Accepted 4 April 2023
Available online 6 April 2023.

(Krabbe-Hartkamp et al., 1998; Kapoor et al., 2008; Shubhangi, 2018). Moreover, it has been also reported that 80% of dysfunctional brains show variants in the circle of Willis, such as at least one missing or underdeveloped artery (Devault et al., 2008). These findings are consistent with research showing that these anatomical variations may affect brain hemodynamics, thus impeding the ability to maintain cerebral perfusion, which in turn represents a potential cerebrovascular risk factor with cognitive implications (Zhu et al., 2015; Pascalau et al., 2019).

As a core component of the medial temporal lobe, and with a critical role in cognition, hippocampal perfusion, in particular, has been correlated with structural integrity (Maass et al., 2015). Differences in arterial supply have also been considered to be involved in the particular hippocampal vulnerability to anoxia and degeneration (Uchimura, 1928; Marinkovic et al., 1992; Davolio et al., 1995; Michaelis et al., 2012). These findings have led to renewed interest in classifying vascular patterns by using *ex-vivo* (Erdem et al., 1993) and *in-vivo* (Spallazzi et al., 2019) techniques. While *in-vivo* assessment prevents potential bias due to *post mortem* changes in arterial calibers (Hyodoh et al., 2012), for a fully non-invasive depiction of the small vessels supplying the hippocampus, the high-resolution capabilities of ultra-high field magnetic resonance imaging (MR) are required (Spallazzi et al., 2019). Congruent results between both *ex-* and *in-vivo* techniques have been obtained according to the different involvement of two main vessels to nurture the hippocampus: the posterior cerebral artery (PCA) and the anterior choroidal artery (AChA).

Based on MR data obtained by high-resolution 7 Tesla (T) Time-of-Flight (ToF) angiography (MRA), it has been shown that the previously mentioned involvement of PCA and AChA presents different and subject-specific qualitative vascular patterns in vivo (Spallazzi et al., 2019). Moreover, it has been proposed that the presence of a mixed blood supply in the hippocampus (receiving branches from both PCA and AChA) in comparison with a single supply (PCA only) is an advantage in several cognitive domains when coexisting with cerebral small vessel disease (CSVD). Furthermore, voxel-based morphometry showed higher anterior hippocampal gray matter volumes in mixed supplied hippocampi (Perosa et al., 2020). More recently, this binary classification (single vs. mixed supply, also called “single vs. dual supply”) has been hypothesized to exert diverse effects in brain structure. For example, differences in gray matter volume have been observed in the anterior hippocampus and entorhinal cortex in relation related to these varied arterial patterns, and further data show that total gray matter volumes are greater in subjects having at least one mixed-supplied hemisphere. These results indicate that different blood supply patterns could have structural implications even beyond the medial temporal lobe (Vockert et al., 2021). Despite this however, no association between CSVD and hippocampal vascularization patterns on gray matter volumes was identified (Vockert et al., 2021). Further complicating this question is the possibility of pattern misclassification. Previous studies, for example, have shown that common methodological constraints, such as motion during scanning, can cause some arterial branches to fall below the detection threshold, which is particularly problematic given the assumption that variations in the contribution of different arteries do not necessarily translate into an increased perfusion (Wiesmann et al., 2020). Moreover, the heterogeneous configuration of the circle of Willis has been described as going beyond merely that of the AChA and PCA (e.g. fetal-like posterior communicating artery), a concern that should also be taken into account (Gutiérrez, 2020). As a result, evidence to support the hypothesis of whether a mixed hippocampal vascularization pattern (accumulative involvement of AChA and PCA) conveys resistance nor resilience against microvascular pathology, remains incomplete.

Given this controversial yet promising state of the art, Vessel Distance Mapping (VDM), with its data-driven approach to vessel patterns and vessel density, provides a novel approach to assess vascularization as a continuous metric instead of an expert decision-based binary classification. In this study, we have applied a novel VDM approach to compare vascular density between (and assess the relationship to cognitive performance in) healthy controls and CSVD patients. We additionally considered supplementary aspects of the circle of Willis, such as vessel diameter and additional arteries, in order to develop a complementary, robust quantitative tool. Building on previous studies (Perosa et al., 2020; Vockert et al., 2021), we applied this method to perform an in-depth analysis of the vascular supply in the hippocampus and its relation to cognition in healthy controls and CSVD subjects. For this purpose, a comparison between VDM and vascular density was performed. Furthermore, the internal correlation among the different VDM-metrics, as well as their association with cognition will be described. Finally, the question of whether this potential interdependence between VDM and cognition varies between healthy subjects and subjects with cerebral microvascular pathology (CSVD) will be addressed.

2. Materials and methods

2.1. Study population

All subjects provided written informed consent according to the Declaration of Helsinki, and the study was approved by the local Ethics Committee (93/17; 28/16). The study was performed using the same cohort as the previously mentioned study of Perosa et al., which included a total of 51 adults. Exclusion criteria included depression, as assessed by the Geriatric Depression Scale (GDS), contraindications for 7T MRI according to the current recommendations of the German Ultrahigh Field Imaging Network (GUFI; https://mr-gufi.de), as well as unrelated neurological pathologies demonstrable by performing physical examinations and cerebrospinal fluid (CSF) analysis. The participants, aged 71 ± 8.5 years (35% females), underwent a 3T MRI (MAGNETOM Verio 3T, Siemens Healthineers, Erlangen, Germany) in the context of a longitudinal study led by the German Center for Neurodegenerative Diseases in Magdeburg (Ethical Approval 28/16), in order to investigate CSVD pathophysiology and its relation to cognition. Presence of CSVD was assessed by a neurologist according to the STRIVE criteria (Wardlaw et al., 2013), and patient inclusion was based on the identification of cerebral microbleeds (CMBs) in lobar or deep or both locations. Of those, 20 participants were diagnosed with CSVD, 8 fulfilled the modified Boston criteria for a possible ($n = 1$) or probable ($n = 7$) cerebral amyloid angiopathy (CAA), while the remaining subjects presented deep or mixed CMBs and were classified as having hyperintensive arteriopathy (Linn et al., 2010; Caetano et al., 2018; Scheumann et al., 2020). Most of the CAA participants underwent a lumbar puncture and presented Alzheimer’s disease (AD) CSF biomarkers available, to which we applied the ATN classification scheme (Jack et al., 2016) according to locally established thresholds: amyloid positivity (A) was analyzed by assessing CSF $A\beta_{1-42}$ levels, tau positivity (T) with CSF phosphorylated-tau levels, and neurodegeneration (N) with total-tau levels. While none of the participants surpassed the thresholds for CSF tau- and neurodegeneration positivity, there were 2 who scored A^+(1 CAA and 1 non-CAA). Therefore, these 2 subjects presented probable AD pathological changes as a part of the AD continuum. Conversely, we recruited healthy control participants from an existing sample of cognitively normal old adults from the DZNE with MRI scans providing iron-sensitive sequences. Those whose imaging did not demonstrate CMBs/cortical superficial siderosis, nor a score above 1 on the Fazekas visual rating scale with respect to white matter hyperintensities, were classified as non-CSVD.

We applied a battery of cognitive tests, including Mini-Mental State Examination (MMSE), Montreal Cognitive Assessment (MoCA), Clinical Dementia Rating (CDR), California Verbal Learning Test II-German version (CVLT-II), and Alzheimer’s Disease Assessment Scale-cognitive subscale (ADAS-cog) to all participants. According to both CDR and MMSE, all control participants and 10 CSVD subjects were classified as cognitively normal, 9 CSVD as mild cognitively impaired ($0 < \text{CDR} \leq 1$; $22 < \text{MMSE} \leq 26$), and 1 fulfilled the criteria for mild dementia (CDR = 0.5, MMSE = 18). No severe dementia was found in any of the subjects (CDR > 1, MMSE ≤ 18).

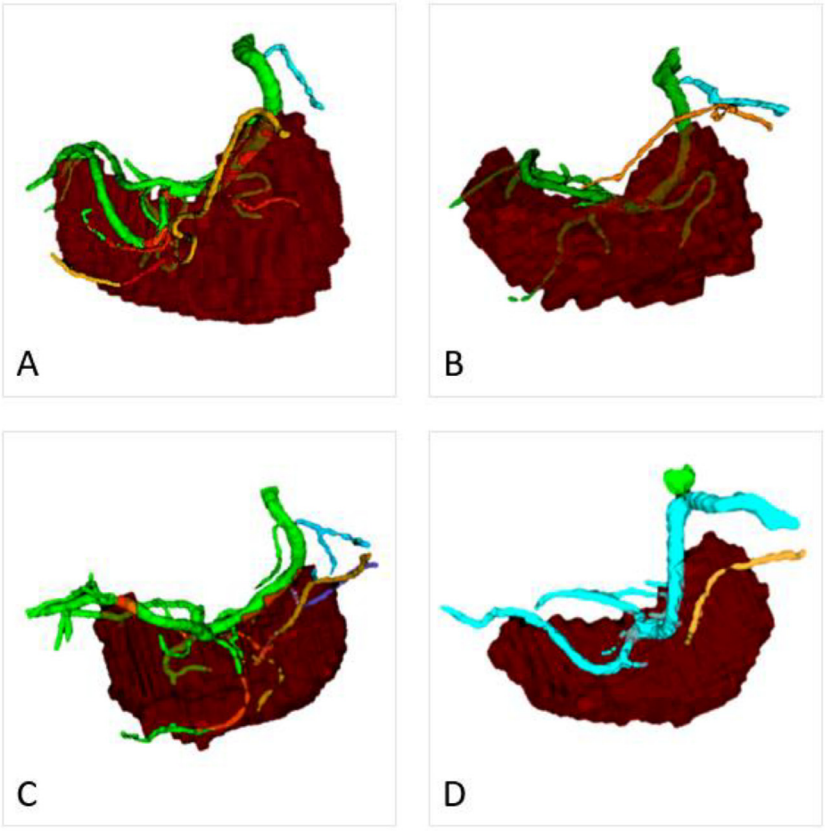

Fig. 1. Three-dimensional rendering of the segmented arteries and hippocampus. In the presented depictions, arteries change color as they enter the hippocampal mask.
A: Hemispheric segmentation of a subject including the hippocampal mask (red), AChA (orange), PCA (green), and PComA (blue). Of note, hippocampal blood supply would be classified as mixed. **B:** Segmentation of a single supplied hippocampus: AChA remains without penetrating the hippocampal mask. **C:** Segmentation of a subject in which an AChA-independent uncal branch (uB, violet, next to AChA and arising from the middle cerebral artery) was found, besides the aforementioned vessels. **D:** Hemispheric segmentation resulting from a fetal-type PComA variant: hypoplastic P1 segment (PCA) with comparatively larger and more predominant PComA.
AChA= Anterior Choroidal Artery; PCA= Posterior Cerebral Artery; PComA= Posterior Communicating Artery, uB= AChA-independent uncal branch.

Furthermore, we acquired 7T arteriographic images (ToF MRA) data from each participant. We analyzed the configuration of the circle of Willis in each hemisphere and participant, in order to determine the number of variants found in the posterior communicating artery (PComA), AChA, and PCA. Participants exhibiting variance in these arteries that could potentially lead to hemodynamic changes large enough to alter the comparability within the sample were excluded ($n = 7$). The number of these variants and their respective types are detailed in the results section, as well as in the supplementary material. A further participant was excluded due to a high incidence of severe head motion during scanning, as were two participants with incomplete cognitive data ($n = 2$). As a result, the final sample size was 41 subjects, aged 70.4 ± 8.6 years (41.5% females). Among them, 15 participants aged 69.3 ± 9.4 years (40% females) were classified as CSVD. Further information regarding study population and scanning protocols can be found in Perosa et al. (2020).

2.2. Arterial segmentation

We scanned all participants with a 7 T MR scanner (Siemens 7 T Classic, Siemens Healthineers, Erlangen, Germany). The protocol included a ToF angiography with 0.28 mm isotropic resolution and sparse venous saturation (Mattern et al., 2018). In brief, the ToF protocol was: echo time/repetition time: 4.59/22 ms; 23° flip angle, bandwidth of 130 Hz/pixel; FoV of 200 × 175x mm with 5 slabs, each 13.44 mm thick and 25% overlap; GRAPPA factor 3, 32 reference lines; acquisition time 18:38 min. The origin of the slab was set at the bottom of the hippocampus and extended approx. 5 cm in the dorsal direction, allowing depiction of the circle of Willis and the hippocampal arteries. Furthermore, structural data were acquired to enable hippocampal segmentation by using FreeSurfer 6.0 (https://surfer.nmr.mgh.harvard.edu) and Automatic Segmentation of Hippocampal Subfields software (ASHS, https://sites.google.com/site/hipposubfields/). While for FreeSurfer, whole hippocampal masks were used, ASHS sub-parcellation into anterior and posterior hippocampus was applied, in order to compare both sets of masks. Per participant, we transformed all masks into ToF space after co-registration of the structural data to the ToF images, and visual inspection ensured proper alignment between the masks and the ToF images.

Subsequently, we used the Multi-Image Analysis GUI software (Mango, http://ric.uthscsa.edu/mango/) to overlay the hippocampal masks onto their respective ToF-images, and we performed manual arterial segmentation in each hemisphere. If depicted in the images, the following four arteries were delineated and labeled per hemisphere individually (Fig. 1):

- Anterior Choroidal Artery (AChA): Segmentation included the AChA's origin at the internal carotid artery and its course within the parahippocampal gyrus to its entry into the choroidal plexus, as well as any of its branches (see Fig. 1, orange label).
- Posterior Cerebral Artery (PCA): Segmentation began in the PCA's origin as the terminal branch of the basilar artery, and included the main trunk in its course from basilar towards occiput, as well as all its branches supplying the temporal lobe. Segmentation was performed along P1 (pre-communicating segment), P2 (post-communicating segment), and P3 (quadrigeminal segment) until P4 (cortical segment), at the division of the medial occipital artery into the occipitotemporal and calcarine branches (see Fig. 1, green label).
- Posterior Communicating Artery (PComA): Segmentation along its entire length from the internal carotid artery to the PCA, including any lateral branch (see Fig. 1, blue label).
- AChA-independent uncal branches (uB): Segmentation along their entire length (see Fig. 1, violet label), as long as they did not constitute any penetrating branch, which has been described to be not related to the medial temporal lobe (Fernández-Miranda et al., 2010).

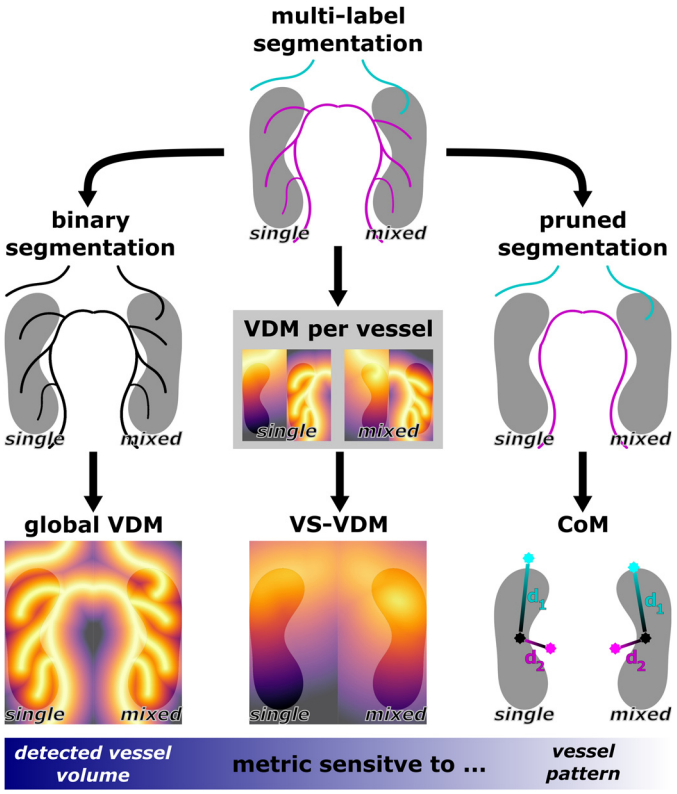

Fig. 2. VDM workflow. Simplified pipeline and metrics overview. Hippocampal single (PCA, purple) and mixed (AChA, blue + PCA) supply patterns are illustrated.
AChA= Anterior Choroidal Artery; CoMD= Center of Mass; PCA= Posterior Cerebral Artery; VDM= Vessel Distance Mapping; VS-VDM= vessel-specific VDM.

Each segmented artery (main trunk and branches) was assigned a distinct numerical label, in order to guarantee subsequent identification during VDM processing. Finally, the areas within and surrounding the hippocampal masks were inspected *a posteriori* to ensure that no arteries in or around the hippocampus remained unsegmented, as much as the aforementioned 7T ToF spatial resolution permitted. Further information regarding the mentioned manual segmentation can be found in Fig. S2.

2.3. Vascular assessment and vessel distance mapping (VDM)

Inspired by previous studies assessing vasculature with respect to its surrounding anatomy by using distances (Haast et al., 2021; Bause et al., 2020; Huck et al., 2019; Bernier et al., 2018), we termed our approach as Vessel Distance Mapping (VDM) (Mattern et al., ESMRMB 2020; Mattern, ESMRMB 2021, ISMRM 2021). Based on vessel segmentation, VDM computes for each voxel the distance to the closest vessel using the Euclidian distance transform. Hence, the binary, sparse vessel segmentation is effectively interpolated, providing a local estimate of the distance to the next surrounding vessel. In contrast, conventional vessel density is computed as the ratio of segmented vessel volume within a region-of-interest (ROI) to the ROI volume itself. Hence, vessel density inherently compresses the regional vascular information into a single number and only considers the relative vessel volume, but not the vascular pattern. With VDM, patterns are approximated by vessel distances, and the following VDM metrics were assessed in this study (Fig. 2):

- *Global VDM* calculates for each voxel how close the nearest vessel is in millimeters. Therefore, global VDM is a proxy for vessel density but also considers vascular spatial patterns. To find the nearest vessel, global VDM considers all segmented vessels. Hence, the nearest vessel is found regardless of its origin (i.e. AChA or PCA).
- *Vessel-specific VDM (VS-VDM)* computes VDM considering each vessel's origin (e.g. AChA) individually. Similar to global VDM, VS-VDM calculates, for each hippocampal voxel, how close the nearest vessel is in millimeters, taking into account that nearest vessel is specific to the AChA or PCA. Therefore, VS-VDM provides more sensitivity with regards to vascular patterns, as distance maps regarding AChA and PCA are computed individually. To combine both maps into a single map, the root-mean-square (RMS) is computed per voxel. Instead of a pure average, RMS is used to penalize long distances. Thus, instead of a binary classification into "single" or "mixed" hippocampal supply, VS-VDM summarizes the closeness and density of both supplying vessels with respect to the hippocampus, into a single, real-valued number:

$$VS-VDM=\sqrt{\frac{VDM_{AChA}{}^2+VDM_{PCA}{}^2}{2}}$$

- *Center of mass distance (CoMD)* was calculated individually for PCA, AChA, and hippocampus. The position of each structure is described by a single point in 3D space, defined by each structure's center of mass, which is in this study equivalent to the center of volume (homogeneous density). For combining these points into a single number, the distances between AChA–hippocampus (d_1) and PCA–hippocampus (d_2) are computed in millimeters and combined by RMS:

$$CoMD=\sqrt{\frac{d_1{}^2+d_2{}^2}{2}}$$

- CoMD represents the computed distances between the hippocampus and AChA's and PCA's respective main trunks. To reduce an excessive sensitivity towards small vessels, the PCA segmentation is pruned before computing the CoMD, to permit that the computed number represents the position of PCA's main trunk, since most of the PCAs were much more highly branched compared to AChA. As a consequence of pruning, sensitivity to vascular density is attenuated, and CoMD estimates the proximity of AChA and PCA to the hippocampus.

The VDM workflow is shown in Fig. 2. Further, the metrics' sensitivity towards the detected vessel volume and the present supply pattern (single or mixed) is illustrated. Global VDM is designed to be sensitive to overall detected vasculature irrespective of its supply origin, while CoMD should be insensitive to the vascular density and only reflect the proximity of the AChA and PCA to the hippocampus. VS-VDM values are sensitive to the proximity and density of AChA and PCA, respectively.

In addition to these three VDM metrics, we computed, per hemisphere, conventional vessel densities and the average PComA and AChA radii. For the vessel radii, the centerline of the vessel segmentation was estimated (skeletonization). Subsequently, for each centerline voxel the shortest distance to the vessel boundary was computed using the Euclidian distance transform. Finally, the radius estimates of all centerline voxels were averaged.

2.4. Statistical analysis

2.4.1. Correlation of vessel density and VDM metrics within the hippocampus for ASHS vs. FreeSurfer masks

Hippocampal segmentation is subject to imperfections. To minimize bias that hippocampal masks may introduce, we estimated the average vessel densities, global VDM, VS-VDM, and CoMD for both the ASHS and FreeSurfer-derived masks. Using Pearson's correlation coefficient, the intra-metric correlations for both mask sets were computed, assuming that if the bias induced by the mask used is low, the metric estimates for ASHS and FreeSurfer-derived masks should correlate.

2.4.2. Relationship between metrics and cognition

We assessed the hypothesized relationship between vessel metrics and cognition with linear regression models. Each metric of interest refers to the mean value of that metric for the bilateral hippocampus. Sex, age, CSVD status, and years of education were included as covariates in the model. For each cognitive test-vessel metric combination, the interaction term of vessel metric and CSVD status, p-value, and R^2 are reported. Additionally, p-values were Bonferroni-corrected to account for multiple testing ($N = 6$; 3 VDM-metrics for each cognitive test: MoCA and ADAS-cog).

This study focused on the results of ADAScog and MoCA. With respect to these, MoCA results presented considerable ceiling effects. As a result, regression quality (represented by R^2) was lower than regression with ADAScog. Hence, the focus of our subsequent analyses lies on ADAScog score as a cognitive measure. Results and plots corresponding to MoCA test outcomes, as well as the results considering additional measures of cognition, are shown in the supplementary material (Fig S1). Furthermore, to supplement understanding of the association among different variables used in the analysis, we calculated correlations for all possible pairs of variables. These included the four covariates, the 17 assessed vessel metrics and the hippocampal vascularization pattern (HVP), which distinguishes participants in which both hippocampi are solely supplied by the PCA from participants with additional hippocampal blood supply via the AChA, as assessed previously (for details see Perosa et al., 2020) resulting in 231 correlation pairs. However, it is important to note that for 4 of the 41 subjects an HVP rating was not available, since a reliable classification of the HVP had not been possible due to vessel pulsation and/or head motion. In details, for these 4 subjects, it was not possible to identify if hyperintense voxels inside the hippocampus and in close proximity to the AChA represented true uncal branch of the artery or image artifacts. Hence, no reliable classification of the HVP (i.e. presence of AChA uncal branch reaching the hippocampus) was possible (Perosa et al., 2020). Nevertheless, the main trunk of the AChA as well as the PCA and its branching was visible and VDM-metrics were computed to increase the sample size. Pairwise correlation coefficients were always calculated on the full available sample, i.e. 37 subjects for all correlations involving the HVP and 41 subjects for all other pairs.

2.4.3. Models: importance of VDM-metrics for cognition

To evaluate the relation of the vessel metrics and cognition and estimate which metric is most strongly related to cognitive outcomes, we compared multiple linear regression models, of the same format as described above. To that end, the previous analysis was extended using additional metrics and hippocampal sub-regions (e.g. anterior vs. posterior masks). ADAScog scores were used as the outcome variable. For each model, one of the following metrics and their interaction term with the CSVD status was considered to predict the test score: vessel densities, global VDM, VS-VDM, CoMD for whole, anterior, and posterior hippocampus, respectively; AChA and PComA radii, respectively; as well as anterior and posterior hippocampal volumes and whole hippocampal volume. The main effect of CSVD was also considered. As in the previous assessment, each metric was averaged bilaterally, and age, sex, CSVD status, and years of education were used as covariates. As shown previously in cross-sectional studies (Perosa et al., 2020; Vockert et al., 2021), if for a participant one or both hemispheres showed a mixed hippocampus supply, i.e. both AChA and PCA contribute, better cognitive performance across several cognitive domains as well as greater total gray matter volumes were observed compared to participants with both hippocampi supplied by the PCA only (single supply). Hence, given the significant correlation across hemispheres, bilateral estimates were averaged (see supplementary material). Further, by bilaterally averaging the VDM metrics per subject, correlation with cognition scores (obtained per subject) was enabled. The explained variance above a baseline model with only covariates allowed a ranking of the aforementioned metrics, and this ranking was used to achieve an approximate comparison of relevance of each metric for cognition. To enable an assessment of the VDM metrics together with the HVP, the supplementary material also includes a section with the same interaction models (plus one for the HVP) in the sample of the 37 participants with HVP. Further, we present an additional approach in the supplementary that takes into account all variables at the same time while enforcing sparsity based on automatic relevance determination.

2.4.4. Data availability

The data that support the findings of this study are available from the corresponding author upon reasonable request.

3. Results

3.1. Hippocampal-focused variations in the configuration of the circle of Willis

A flow chart of the enrolled study population with variations considered in the configuration of the circle of Willis, as well as participants included in the statistical analysis can be found in Fig. 3. Additional information is included in Table S1.

From a total of 51 7T-MRI-ToF scanned participants, PComA was found to be absent/severely hypoplastic in 30 participants ($n = 9$ bilaterally, $n = 21$ unilaterally), among whom 10 were diagnosed with CSVD. Among the latter, 60% ($n = 6$) corresponded to participants with bilateral absence/severe hypoplasia of PComA. In turn, 78% of participants with absence/severe hypoplasia of PComA ($n = 7$) were classified as having CSVD. Conversely, 21 participants showed the classical configuration: a closed ring-like circle of Willis (PComA present in both hemispheres).

Additional observed variants were fetal-like PComA ($n = 5$), PCA's unilateral absence without PComA's compensation ($n = 1$), and the apparent involvement of the superior cerebellar artery in the region of interest ($n = 1$), all of which were excluded from the statistical analysis due to their potential confounding influence in our relatively small sample. Participants whose images presented intense motion artifacts that reduced the confidence of the arterial segmentation ($n = 1$) or without available cognitive results ($n = 2$) were excluded as well. Therefore, 10 participants were excluded from the subsequent data analysis. As a result, 41 participants were included for the statistical analyses, considering cognition, covariates, vessel radii, and VDM-metrics as provided by the segmentation of PCA, AChA, and PComA. Unilateral AChA-independent uncal branches (uB) close to the hippocampus were found only in 5 participants, all of them arising from the internal carotid. No bilateral supply through these vessels was found. Due to its reduced sample size, uB was not considered in the VDM evaluations.

3.2. Intra-metric correlations: ASHS vs. FreeSurfer hippocampal masks

To assess possible effects of hippocampal mask bias on vessel metrics, for each metric individually, vessel densities and the three previously described VDM metrics obtained for ASHS masks were correlated with those obtained with the FreeSurfer masks. For vessel densities, we observed a Pearson's correlation coefficient of 0.34 (p_{Bonf}-value = 0.0024). Hence, vessel density estimates computed for different hippocampus masks correlate only slightly with each other. Therefore, over- or underestimation of the hippocampal volume, depending on the mask used, could induce considerable bias in the computed vessel densities, reducing the metrics' robustness. Conversely, the intra-metric correlation showed strong (Pearson's correlation coefficient $r>0.9$) and significant ($p_{Bonf}<0.001$) values for the global VDM ($r = 0.90$), VS-VDM ($r = 0.94$), and CoMD ($r = 0.92$).

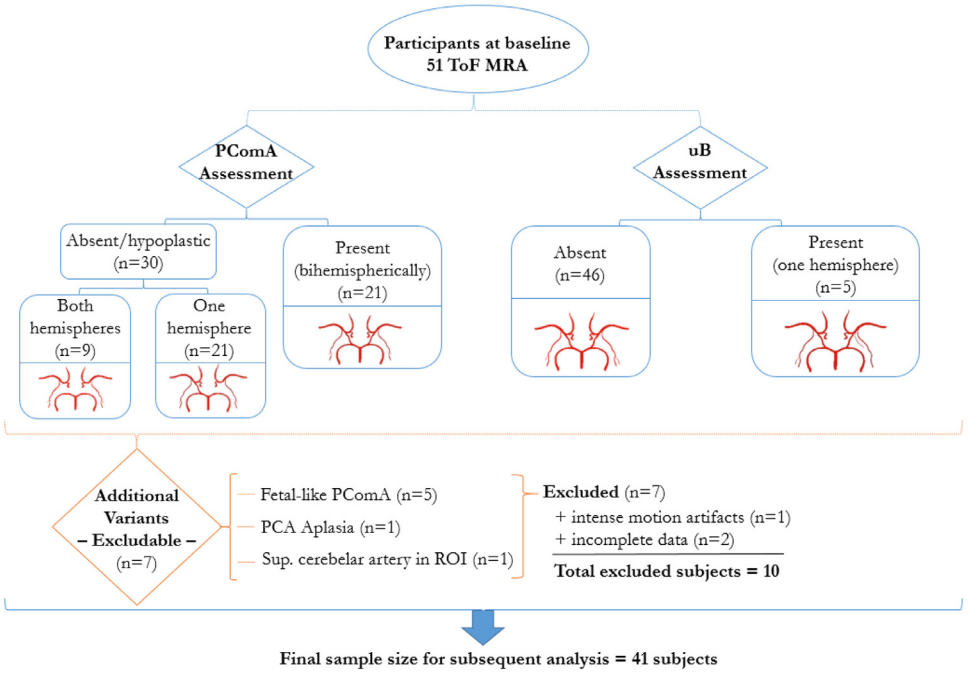

Fig. 3. Simplified flowchart of the enrolled study population regarding variants and excluded subjects.

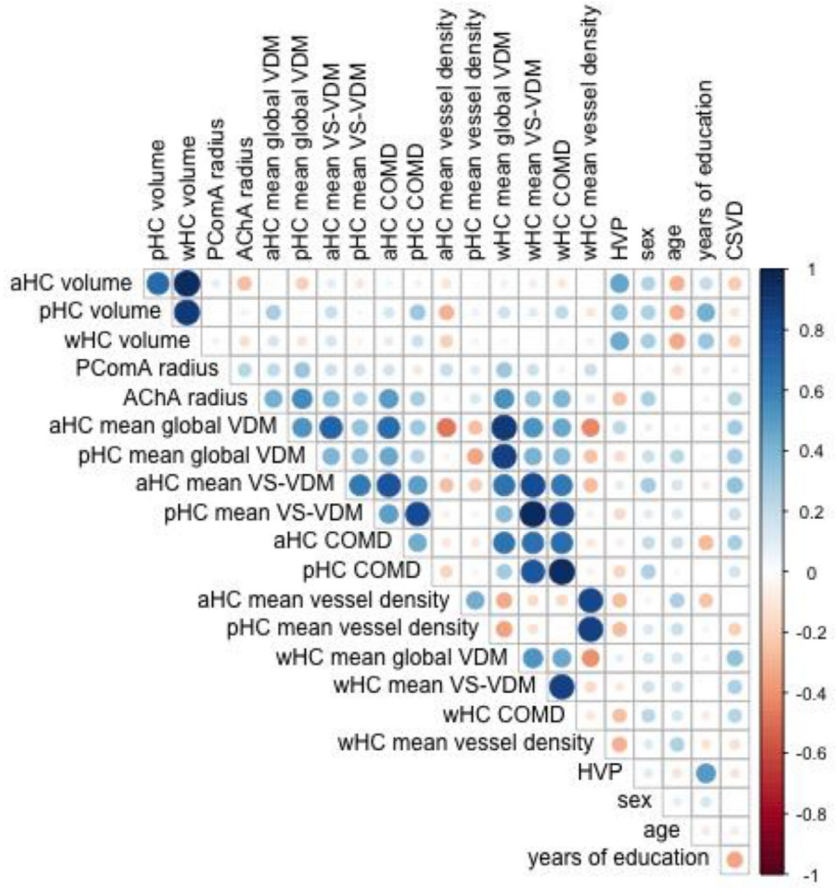

Fig. 4. Correlation among vessel metrics and covariates. Circle size denotes the strength of the correlation. Circle color represents the r value according to the color bar, thus including additional information about the direction of the correlation. Please note that all pairwise correlations are calculated on the maximum possible available sample, i.e. 37 subjects for correlations involving the HVP and 41 subjects for all other pairs. AChA= Anterior Choroidal Artery; aHC= anterior hippocampus; CoMD= Center of Mass Distance; HVP = hippocampal vascularization pattern; PComA= Posterior Communicating Artery; pHC= posterior hippocampus; VDM= Vessel Distance Mapping; VS-VDM= Vessel-Specific VDM; wHC= whole hippocampus.

3.3. Correlation among metrics

An overview of all correlations is shown in Fig. 4 and the exact r values of all 210 metric pairs can be found in the supplementary along with their p-values.

When correlating different metrics within the same region of interest (ROI), estimates for VS-VDM and CoMD correlated with each other for the whole (r = 0.8499), anterior (r = 0.7790), and posterior hippocampus (r = 0.8184), respectively. Furthermore, VS-VDM correlated notably with global VDM values for the whole hippocampus (r = 0.7092) and anterior hippocampus (r = 0.5268), while correlations for CoMD vs.

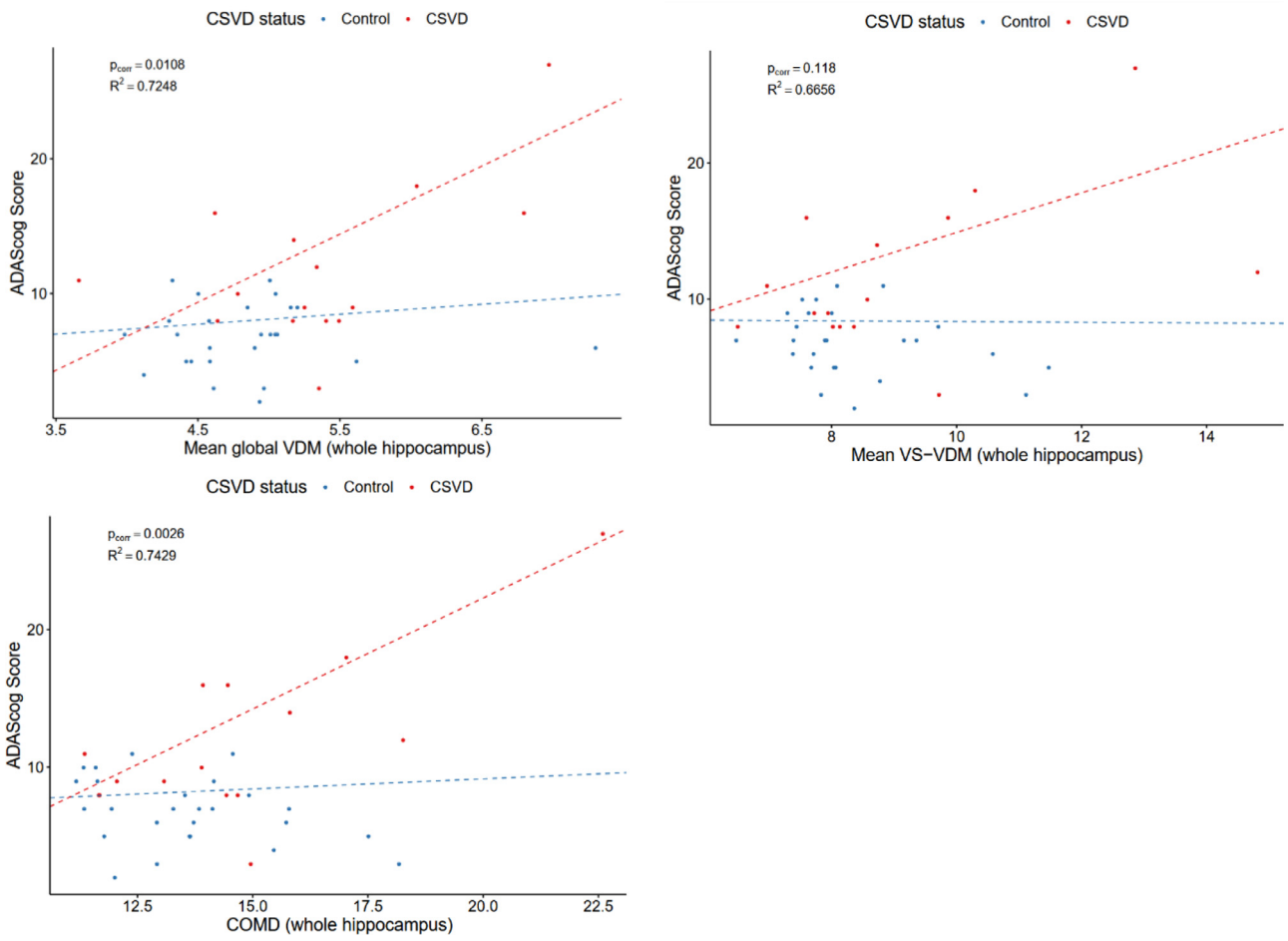

Fig. 5. Correlation between cognitive status (ADAScog scores) and VDM metrics (cognitive status vs. mean global VDM; cognitive status vs. mean VS-VDM; cognitive status vs. CO MD).
The sample was divided between controls (blue) and CSVD (red). The p value refers to the (Bonferroni-adjusted) p value of the interaction term between CSVD and the respective VDM metric in the corresponding linear regression model, R^2 values to the whole model.
ADAScog= Alzheimer's Disease Assessment Scale-Cognitive Subscale; CoMD= Center of Mass Distance; VDM= Vessel Distance Mapping; VS-VDM= vessel-specific VDM.

global VDM only exceeded 0.5 for the anterior hippocampal estimates (r = 0.6378). When considering the same region of interest (e.g. whole, anterior, or posterior hippocampus), correlation of vessel densities with other metrics never exceeded 0.5. Therefore, the observed correlations were strongest for intra-metric (same VDM-metric across different ROIs) comparisons, while inter-metric correlation was strongest for VS-VDM vs. CoMD. The volumes of the anterior (aHC) and posterior hippocampus (pHC) were also correlated in this cohort (r = 0.6853). In turn, the volume of the whole hippocampus (wHC) showed high correlations with aHC volume (r = 0.9455) and pHC volume (r = 0.8851). Regarding VDM-metrics, CoMD in the wHC was also highly correlated with CoMD in the pHC (r = 0.8851). Correlation of a reported metric and the covariates (age, sex, education, and CSVD status) exceeded 0.5 only for the pair of HVP and years of education (r = 0.5026; see Fig. 4). Further information about the correlations can be found in the supplementary material.

3.4. Association of VDM-metrics with cognition

In order to assess the relationship between three VDM-metrics and cognitive performance cognition, the previously described linear regression models were applied. Due to the aforementioned bias towards the hippocampal mask, vessel densities were omitted.

Fig. 5 suggests that the observed increased values of CoMD, global, and VS-VDM for the whole hippocampus were related to higher ADAScog scores (worse cognitive outcomes) for CSVD subjects, while no such association can be observed in healthy controls. As a surrogate for resilience, we assessed the interaction term of CSVD status and the metric of interest, resulting in a significant interaction with CoMD (R^2=0.7429; p_{Bonf}-value = 0.0026). The R^2 value indicates that the model explained 74.29% of the ADAScog score's variance. The explained variance for the global VDM was slightly lower, but retained statistical significance (R^2=0.7248; interaction effect: p_{Bonf}-value = 0.0106). For the VS-VDM, the interaction term did not meet a statistically significant threshold (p_{Bonf}-value=0.118), while still, however, yielding a considerable R^2-value (0.6656).

The same analysis was performed for the MoCA score (Supplementary Material). The overall explained variance was lower (52–58%) and only the interaction of CSVD status with CoMD showed a strong trend after correcting for multiple testing (p_{Bonf}-value = 0.0701). Arguably, the observed ceiling effects in the MoCA score may have contributed to this reduction in the explained variance, suggesting the ADAScog as a more suitable test for the regression model comparison.

To provide the reader with a more complete picture, the same scatter plots for the MMSE and CVLT can be found in the Supplementary Material. However, please note that the scores of all four cognitive tests are highly correlated ($r > 0.75$ or $r < -0.75$). We further conducted a sup-

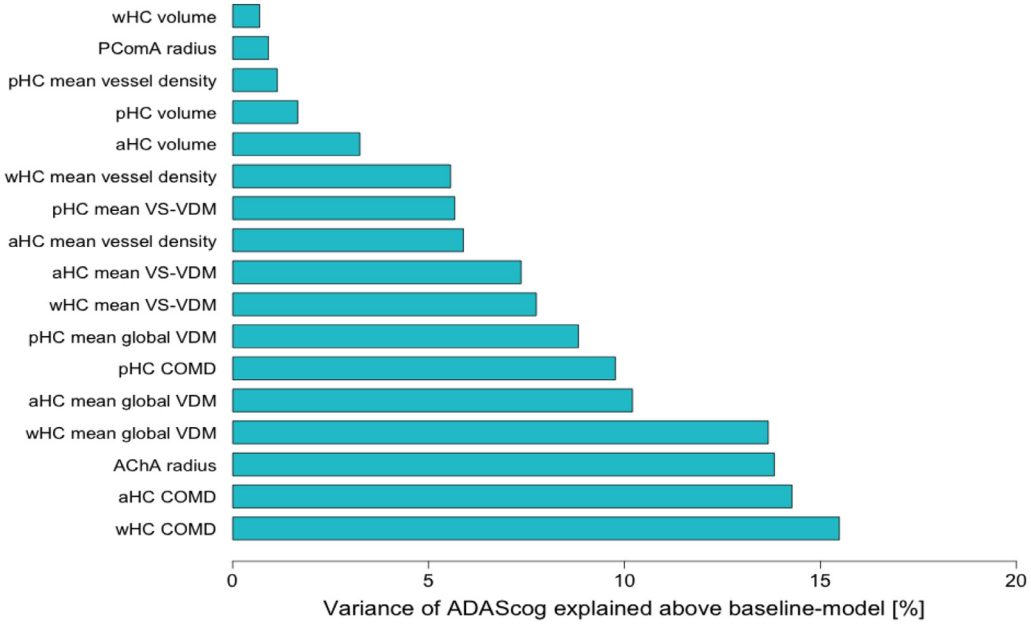

Fig. 6. Importance ranking of vessel- and VDM-metrics. The metrics are ranked by the amount of additional variance in ADAS-cog scores they explain above the baseline model. Baseline model contained age, sex, education years, and CSVD status as covariates. Full models each contained an additional term for the metric and for the interaction of the metric with CSVD.
AChA= Anterior Choroidal Artery; aHC= anterior hippocampus; CoMD= Center of Mass Distance; PComA= Posterior Communicating Artery; pHC= posterior hippocampus; VDM= Vessel Distance Mapping; VS-VDM= Vessel-Specific VDM; wHC= whole hippocampus.

plementary analysis for the ADAScog and MoCA excluding participants more than 3*SD from the mean of a given metric (see also Supplementary Material).

3.5. Ranking of vessel- and VDM-metrics

With the aim of addressing the specific importance of the estimated vessel- and VDM-metrics, we performed regression models with ADAScog as the outcome variable, including the vessel metrics, their respective interaction with the CSVD score, and the other aforementioned covariates. Thus, the cognitive score was predicted with a model including the covariates (fixed term), the variable of interest (changing term) and its interaction with CSVD. Results obtained from these models, which changed according to the variable of interest, allowed us to estimate the differing impact of each variable on cognition, when compared with a baseline model (which merely included the four covariates). Therefore, models were ranked by the amount of explained variance to estimate their relevance for predicting the cognitive outcome. The results are shown in Fig. 6.

The R^2 for the baseline model was 0.5881, while the full model including the bilaterally averaged CoMD in the whole hippocampus returned the highest R^2 with 74.29% of the ADAScog's variance explained (considering covariates, CoMD, and the interaction of CoMD and CSVD status). Comparing the percentages obtained according to the R^2 values only for vessel metrics per region of interest (anterior, posterior, and whole hippocampus, respectively) provided the following ranking: 1. CoMD (73.08%, 68.58%, 74.29%), 2. global VDM (69.01%, 67.63%, 72.48%), 3. VS-VDM (66.17%, 64.48%, 66.56%), and 4. vessel density (64.70%, 59.95%, 64.37%).

Whole hippocampal scores explained more variance in cognition than anterior hippocampal scores. Moreover, anterior hippocampal estimates explained more variance than the posterior ones. In addition, the anterior hippocampal volume returned higher percentages than the posterior volume (62.05% vs. 60.47%) while only three other metrics returned a lower R^2: wHC volume, PComA radius, and posterior vessel density. In contrast, bilateral AChA radius also returned one of the highest R^2 with 72.63%, compared to its counterpart (59.72% for the bilateral PComA radius, second lowest R^2).

The distance between the center of mass for the two supplying branches (AChA and PCA's main trunk) to the hippocampus was the metric explaining the highest variance in cognition, followed by the AChA radii and the global hippocampal VDM, respectively. In contrast, posterior-specific measures returned lower R^2 values relative to their anterior or whole hippocampal counterparts. Interestingly, hippocampal volumes explained less variance than the VDM-metrics, showing a predominance of vessel-metrics over structural MR measures.

Additional comparisons of interaction models including HVP as well as an automatic relevance determination to jointly model all metrics are presented in the supplementary material. Overall, all model approaches showed similar trends and agreed on the high relevance of CoMD to predict cognition. Differences in the ranking of the metrics are likely caused by model-specific selection criteria (i.e. sparsity enforced by the automatic relevance determination) and different sample sizes (i.e. $n = 37$ for the models with HVP). Comparisons in the supplementary material indicate the previously introduced expert-based HVP rating provides complementary information to the here presented VDM approach, requiring follow-up investigations. Detailed discussion of the results and ranking obtained for all modeling approaches is provided in the supplementary material.

4. Discussion

In this study, we investigated different arterial parameters involved in hippocampal blood supply and their potential correlation with cognition in a cohort of older adults using a novel vessel distance mapping (VDM) approach. To our knowledge, this work is the first in which hippocampal vascularization patterns were assessed in vivo with continuous metrics instead of binary classifications previously described in the literature. To that end, this VDM framework provides an in-depth analysis of the vasculature detected in high resolution imaging, and additionally considers previously overlooked vessels (initially PCom and AChA-independent uncal branches) and hippocampal subregions. With the proposed analysis, we addressed the question of whether different

vessel metrics are related to cognition and which of these metrics is the most relevant for explaining variance in cognition. Thus, we assessed the relevance of vascular patterns, vessel density, and vessel radii for potential cognitive resilience mechanism. As a result, our approach of using both structural MR images and VDM allows the non-invasive investigation of the interdependency between brain vasculature and cognition. Further, by combining VDM-derived metrics with multi-label vessel segmentation (Dumais et al., 2022) a fully automatic vessel pattern assessment could be realized in the future.

4.1. Vascular patterns, VDM, and cognition

The hippocampus as a critical and highly interconnected hub that contributes to fundamental cognitive domains such as perception, navigation, and episodic memory (Zeidman et al., 2016; Lisman et al., 2017; McDonald et al., 2017). It is also positioned as an interface between the anterior (originating from the carotid artery) and posterior (vertebrobasilar) circulation systems deploying the circle of Willis (Erdem et al., 1993; Tatu et al., 2014). We hypothesized, given recent findings (Perosa et al., 2020; Vockert et al., 2021) that arterial variations in this area, which transcend sex and ethnicity (Eftekhar et al., 2006; Hashemi et al., 2013; Hindenes et al., 2020) and are present in over half of the general population (Fisher, 1965; Kapoor et al., 2008; Jones et al., 2021) would result in variation in cognitive outcomes. Furthermore, these variations have been associated with numerous cerebrovascular diseases (Chuang et al., 2008; Silva Neto et al., 2012; Henry et al., 2015), as the symmetric anastomotic arterial network of a closed ring-like circle of Willis has been proposed to provide a collateral circulation that assists in the prevention of brain transient ischemia and stroke (Hoksbergen et al., 2000a, 2003; Karatas et al., 2015; Pascalau et al., 2019). In this context, findings show that most anatomical variation occurs in the posterior part of the circle of Willis, specifically in the PComA, where hypoplasia is the most common finding (Kapoor et al., 2008; Karatas et al., 2015). Since standard and bilateral conservation of the posterior circulation in the circle of Willis has been linked to memory function (Barba et al., 1997; Zijlmans et al., 2012; Altinbas et al., 2014), arterial radii were included in this work. Accordingly, in order to ascertain the role that PComA radius might play as a key collateral pathway between the two possible sources (AChA and PCA) of hippocampal blood supply in our sample, its average values were included. However, this resulted in the second lowest amount of explained variance for predicting cognition, according to ADAScog outcomes. Moreover, there was no observed correlation with the hippocampal volumes, nor with VDM metrics. In contrast, AChA radius was one of the variables that explained the greatest amount of variance in cognition, and showed higher correlations with VDM metrics. This phenomenon reaches a maximum for global VDM, which, in turn, shows significant correlations with VS-VDM and with CoMD in the hippocampus, with the latter being the most relevant factor for explaining variance in ADAScog results. Furthermore, interaction model comparison (full sample, $n = 41$)and automatic relevance determination showed that VDM metrics in more posterior regions of the hippocampus were less relevant for predicting cognitive outcomes, which is consistent with observations that higher anatomical variability in the hippocampal vascularization is more anterior, as AChA's contribution is greater than the PCA's (Spallazzi et al., 2019). The overall trend across all model approaches indicated CoMD of the whole and anterior hippocampus as the most relevant metric. Only the interaction models with HVP ($n = 37$) assigned slightly higher relevance to the whole and posterior global VDM (less than 2% increase compared to CoMD), likely caused by the subsample used. The tendency of a lower cognitive association when considering the posterior hippocampus (dominantly supplied by PCA), combined with the relevance of metrics sensitive to the AChA (e.g. CoMD and AChA radius), suggests that arterial supply patterns are relevant for cognitive function only when coexisting with CSVD. Hence, a pattern-based resilience mechanism appears to be plausible.

Global VDM computes the minimal distance between a voxel and its closest vessel, which quantifies the overall detected vasculature in and surrounding the hippocampus. This VDM-metric seems to be of relevance as well (relevance rank compared to other metrics depends on the modeling approach and sample size used). In addition to the classical concept of vessel density, global VDM is highly sensitive to the number of detected vessels. However, and unlike classical vessel densities, an AChA close to, but not entering the hippocampus, will decrease global VDM estimates in the anterior hippocampus. Hence, global VDM (vessel density surrogate), VS-VDM (arterial AChA-PCA-dependent supply patterns), and CoMD (revealing distances among the hippocampus and AChA's and PCA's respective main trunks) have varying sensitivity in different aspects of the detected vessel trajectories. In this cohort, we report that a mixed contribution of vascular supply pattern and vessel density is suspected to contribute to resilience (Montine et al., 2019; Stern et al., 2019) in CSVD, particularly as we observed that increased values of CoMD, global-VDM, and VS-VDM (reflecting longer distances among the arteries) correlated with higher ADAS-cog scores for CSVD (poorer cognition). In contrast, we did not observe such an association in our healthy controls. These findings raise the question of whether the presence of PComA would also play an essential role in the presence of vascular pathology in specific locations, e.g. the internal carotid (specially at segments that are more proximal than C4) or the proximal PCA. In this context, the finding that a majority of participants who presented bilateral absence or hypoplasia of PComA also had CSVD ($n = 7$ out of 9) should not be considered trivial. Unfortunately, however, our comparatively small sample size limited further sub-analysis focusing on CSVD's regional distribution.

Anatomical variations in terms of the presence or absence of certain vessels has also offered controversial results with respect to their involvement in brain ischemia and poorer cognitive outcomes in stroke patients (Oumer et al., 2021; Westphal et al., 2021). In this sense, additional metrics provided by VDM could be useful in predicting cognitive outcomes in relation to baseline vascular risk, irrespective of which vessels are involved. Global VDM and VS-VDM also provide the additional advantage of interpolating the inherently sparse vessel information, as an alternative to mere vessel densities.

4.2. Study limitations, clinical translation, and future work

There are, however, some limitations which should be considered when interpreting these findings. Firstly, the sample size of this study was relatively constrained, requiring further studies to replicate these findings in larger samples. Secondly, MRI-related partial volume averaging (González Ballester et al., 2002; Peh, 2014) and resolution limits could have introduced a bias in the depiction, segmentation, and quantification of very thin and small arteries. It should also be noted that VDM and vessel densities are both limited to the segmented vessels, also known as resolution dependency. Hippocampal arteries have been described to measure 0.28 to 0.8 mm (Marinković et al., 1992) with mean values of 0.48 mm (hippocampal head), 0.59 mm (hippocampal body), and 0.43 mm (hippocampal tail). Therefore, most of these vessels are expected to exceed the spatial resolution employed in our study. Resolution dependency may be of particular relevance with regard to the AChA, since its diameter gets progressively reduced in an anterior-posterior direction along its longitudinal axis. This might drive some of the observed differences in anterior vs. posterior VDM metrics because the posterior part of the AChA might be not visible in all images. However, as the AChA progresses posterior in direction its trajectory diverges from the hippocampus, while the PCA's branches enter the hippocampus more towards the posterior part of the hippocampus. Hence, differences in anterior vs. posterior VDM estimates are expected to be driven by vessel anatomy. Additionally, no correlation between AChA radii and centerline length was found (Fig. S6). Nevertheless, the resolution, manual segmentation (performed on a voxel-by-voxel basis; see

Fig. S2) and the variable inflow enhancement represent residual sources of bias in this study.

As mentioned above, we segmented the anterior and posterior uncal branches from the AChA as well as the AChA-independent uncal branches. However, the sample size containing the latter was not large enough to provide statistical confidence. The same is true for fetal-like PComA variants (observed as a predominance of PComA over PCA, whose P1 segment showed aplasia or hypoplasia): they were found in approximately 10% of our scanned population (n = 5), in a manner consistent with the 7–30% range described in the literature (Krabbe-Hartkamp et al., 1998; Hoksbergen et al., 2000b; Jongen et al., 2004; de Caro et al., 2021). We also consider them worthy of further assessments, given that they have been suggested to increase the severity of stroke (Shaban et al., 2013; Di Pietro et al., 2021), as well as their correlation with lower cognitive performance when interventional procedures at the internal carotid are performed (Zijlmans et al., 2012). However, research has shown contradictory results regarding the association between these variants and an increased risk of brain infarction (Capone et al., 2019). In our study, the vast majority of participants presenting this variant were affected by CSVD (4:1), possibly reflecting an increased risk of fetal-like PComA towards vascular insult. Whether fetal-like PComAs should be considered as a mixed pattern of hippocampal supply or a single pattern of supply, as well as if there are hemodynamic implications reflected by specific VDM-metrics in these cases should be addressed in future studies.

Moreover, there were 2 participants whose CSF-makers surpassed the thresholds for Aβ 1–42, hence scoring as $A+$ to the ATN classification proposed by Jack et al. (2016). Therefore, we cannot rule out the possibility of AD pathological changes in these participants. Given the limitations of our sample size, the complex association among VDM, CSVD, cognition, and senile plaques under both standard and special configurations of the circle of Willis, is still to be investigated in a specifically designed study. We also acknowledge that in the present work, as a cross-sectional study, causality from the mentioned arterial metrics towards cognition cannot be determined, and reverse causality cannot be excluded. However, it is not the purpose of this paper to highlight the quantity of arterial blood supply as an isolated element promoting cognition, but VDM-metrics as a tool reflecting additional vascular aspects (e.g. arterial patterns). These aspects could provide further evidence of resilience being a confluent circumstance, which requires the involvement of several conditions rather than exclusive reliance on a single factor. Importantly, vascularization patterns exhibiting more and closer vessels do not necessarily lead to additional perfusion, but could instead represent a way for guaranteeing blood flow in spite of vascular pathology.

The relationship between vascular patterns, VDM, and perfusion are topics to be assessed in future studies. Previously introduced hippocampal vascularization patterns (binary classification) seem to provide complementary information to the here presented VDM approach (continuous metrics) with similar levels of relevance to explain variance observed in cognition scores (see supplementary material). While in particular CoMD was inspired by the expert-based pattern rating, it is no one-to-one translation, i.e. CoMD considers the PCA and AChA distance to the hippocampus while the HVP is an expert rating of the expected AChA contribution to the hippocampal blood supply and does not consider the PCA. Future investigations are required to understand the complementary nature of both approaches comprehensively to enable more precise predictions and, in combination with deep learning-based multilabel vessel segmentation, a fully automatic hippocampal vascularization assessment. Further, given that VDM allows for the evaluation of the vessel structure from high resolution ToF angiography, this could be combined with ASL-based perfusion data to study the structure and function of the hippocampal vascularization at the mesoscopic scale (Haast et al., 2021). Additionally, VDM uses the distance between a voxel and a vessel to estimate the vessel's relevance in the blood supply, without measuring vessel territories directly. The pure structure-driven approach in VDM is motivated by the fact that with decreasing vessel size, the vessel territory becomes smaller and more spatially specific, until it can be approximated by an ellipsoid (Feekes et al., 2006). Validation through non-invasive vessel territory imaging should be a focus of future studies (Hartkamp et al., 2013; Zhang et al., 2021).

In addition, besides vascular distances, densities, and (resting) perfusion, vascular reactivity is an essential for the functional integrity of the brain. Vascular reactivity defines wall tension, resistance, tone, blood flow, and ultimately vascular response to metabolic demand (Nurkiewicz et al., 2010; Losordo et al., 2016). Maintaining the delicate balance of these factors impacts on neurological recovery in the event of a stroke (Zheng et al., 2022), and it is also known to be disrupted in CSVD and in cognitive impairment (Cannistraro et al., 2019; Bär et al., 2007; Xu et al., 2022). Potentially, in coexistence with disease, hippocampal perfusion might be mediated by vascular patterns and vascular reactivity. Thus, future studies are required to understand the interdependence of vascular structure, perfusion, vascular reactivity, and ultimately cognition.

Regarding the reproducibility and potential implications of our findings, neuroimaging at 7T would provide greater signal-to-noise ratio at similar faster scan times compared with 1.5T and 3T scans, thus allowing for a more fine-grained investigation with VDM (Jones, 2021). It is also worth noting the clinical utility of using 3T scanners as field strengths range from 1.5. to 3 T in clinical settings (Wardlaw et al., 2012). Since CoMD (based on the AChA's and PCA's main trunks) was the VDM-metric with the highest relation to cognition, any imaging modality with the capability to depict the arteries of interest could be used. Therefore, 7T is not necessarily required to reproduce the results obtained from this study. Given that the AChA and PCA can be detected at clinically available field strengths, considerable translational potential for the approach presented here exists and should be further assessed in future studies.

5. Conclusions

VDM provides continuous metrics to characterize vascular patterns on a spectrum instead of traditional binary classifications and extends beyond ROI-wise density estimates, allowing for greater investigation of hippocampal vascularization with promising clinical applications. Furthermore, VDM is useful for establishing vessel-specific metrics with reduced bias towards hippocampal mask generation compared to vessel densities. Our results show that VDM-metrics applied to the hippocampus considering general and specific vessels and their patterns can offer a way to depict vascular resilience. Notably, VDM-metrics were correlated with higher amounts of explained variance in the cognitive outcomes of subjects suffering from CSVD, with several potential implications in clinical applications and research, providing a much needed platform for planning future studies.

Declaration of Competing Interest

The authors declare no conflicts of interest.

Credit authorship contribution statement

Berta Garcia-Garcia: Conceptualization, Methodology, Visualization, Writing – original draft. **Hendrik Mattern:** Conceptualization, Software, Methodology, Writing – original draft. **Niklas Vockert:** Methodology, Validation, Formal analysis, Writing – review & editing. **Renat Yakupov:** Validation, Software. **Frank Schreiber:** Software, Data curation. **Marco Spallazzi:** Writing – review & editing. **Valentina Perosa:** Writing – review & editing. **Aiden Haghikia:** Supervision, Project administration. **Oliver Speck:** Supervision, Writing – review & editing. **Emrah Düzel:** Supervision, Funding acquisition. **Anne Maass:** Supervision, Writing – review & editing. **Stefanie Schreiber:** Supervision, Writing – review & editing.

Data availability

Data will be made available on request.

Acknowledgements

The project leading to this article has been supported by the German Research Foundation (DFG, 9th Nachwuchsakademie Medizintechnik, MA 9235/1-1; Project-ID 425899996/TPB04 SFB 1436; and CRC 779, TP A07) and the BMBF EnergI-Consortium (TP01).

Supplementary materials

Supplementary material associated with this article can be found, in the online version, at doi:10.1016/j.neuroimage.2023.120094.

References

Altinbas, A., Hendrikse, J., Algra, A., van Zandvoort, M.J., Brown, M.M., Bonati, L.H., de Borst, G.J., Kappelle, L.J., van der Worp, H.B., 2014. Ipsilateral foetal-type posterior cerebral artery is associated with cognitive decline after carotid revascularisation. BMC Neurol. 14, 84.

Bause, J., Polimeni, J.R., Stelzer, J., In, M.H., Ehses, P., Kraemer-Fernández, P., Aghaeifar, A., Lacosse, E., Pohmann, R., Scheffler, K., 2020. Impact of prospective motion correction, distortion correction methods and large vein bias on the spatial accuracy of cortical laminar fMRI at 9.4 Tesla. Neuroimage 208, 116434. doi:10.1016/j.neuroimage.2019.116434.

Bär, K.J., Boettger, M.K., Seidler, N., Mentzel, H.J., Terborg, C., Sauer, H., 2007. Influence of galantamine on vasomotor reactivity in Alzheimer's disease and vascular dementia due to cerebral microangiopathy. Stroke 38 (12), 3186–3192. doi:10.1161/STROKEAHA.107.492033.

Bernier, M., Cunnane, S.C., Whittingstall, K., 2018. The morphology of the human cerebrovascular system. Hum. Brain Mapp. 39 (12), 4692 -495.

Binnewijzend, M.A.A., Benedictus, M.R., Kuijer, J.P.A., van der Flier, W.M., Teunissen, C.E., Prins, N.D., Watjes, M.P., van Berckel, B.N.M., Scheltens, P., Barkhof, F., 2016. Cerebral perfusion in the predementia stages of Alzheimer's disease. Eur. Radiol. 26, 506–514.

Barba, G.D., Boissé, M.F., Bartolomeo, P., Bachoud-Lévi, A.C., 1997. Confabulation following rupture of posterior communicating artery. Cortex 33 (3), 563–570.

Caetano, A., Ladeira, F., Barbosa, R., Calado, S., Viana-Baptista, M., 2018. Cerebral amyloid angiopathy – The modified Boston criteria in clinical practice. J. Neurosci. 384, 55–57.

Cannistraro, R.J., Badi, M., Eidelman, B.H., Dickson, D.W., Middlebrooks, E.H., Meschia, J.F., 2019. CNS small vessel disease: a clinical review. Neurology 92 (24), 1146–1156.

Capone, S., Shah, N., George-St Bernard, R.R., 2019. A fetal-type variant posterior communicating artery and its clinical significance. Cureus 11 (7), e5064.

Chuang, Y.M., Liu, C.Y., Pan, P.J., Lin, C.P., 2008. Posterior communicating artery hypoplasia as a risk factor for acute ischemic stroke in the absence of carotid artery occlusion. J. Clin. Neurosci. 15 (12), 1376–1381.

Davolio, C., Greenamyre, J.T., 1995. Selective vulnerability of the CA1 region of hippocampus to the indirect excitotoxic effects of malonic acid. Neurosci. Lett. 192 (1), 29–32.

De Caro, J., Ciacciarelli, A., Tessitore, A., Buonomo, O., Calzoni, A., Francalanza, I., Dell'Aera, C., Cosenza, D., Currò, C.T., Granata, F., Vinci, S.L., Trimarchi, G., Toscano, A., Musolino, R.F., La Spina, P., 2021. Variants of the circle of Willis in ischemic stroke patients. J. Neurol. 268 (10), 3799–3807.

Devault, K., Gremaud, P.A., Novak, V., Olufsen, M.S., Vernières, G., Zhao, P., 2008. Blood flow in the circle of Willis: modeling and calibration. Multiscale Model. Simul. 7 (2), 888–909.

Di Pietro, M., Di Stefano, V., Cannella, R., Di Blasio, F., De Angelis, M.V., 2021. Fetal variant of posterior cerebral artery: just a physiologic variant or a window for possible ischemic stroke? Neurol. Sci. 42, 2535–2538.

Dumais, F., Caceres, M.P., Janelle, F., Seifeldine, K., Arès-Bruneau, N., Gutierrez, J., Bocti, C., Whittingstall, K., 2022. eICAB: a novel deep learning pipeline for Circle of Willis multiclass segmentation and analysis. Neuroimage 260, 119425. doi:10.1016/j.neuroimage.2022.119425.

Düzel, E., Van Praag, H., Sendtner, M., 2016. Can physical exercise in old age improve memory and hippocampal function? Brain 139, 662–673.

Eftekhar, B., Dadmehr, M., Ansari, S., Ghodsi, M., Nazparvar, B., Ketabchi, E., 2006. Are the distributions of variations of circle of Willis different in different populations? - Results of an anatomical study and review of literature. BMC Neurol. 6, 22.

Erdem, A., Gazi Yasargil, M., Roth, P., 1993. Microsurgical anatomy of the hippocampal arteries. J. Neurosurg. 79, 256–265.

Feekes, J.A., Cassell, M.D., 2006. The vascular supply of the functional compartments of the human striatum. Brain 129 (8), 2189–2201.

Fernández-Miranda, J.C., de Oliveira, E., Rubino, P.A., Wen, H.T., Rhoton, A.L., 2010. Microvascular anatomy of the medial temporal region: part 1 - its application to arteriovenous malformation surgery. Oper. Neurosurg. 67 (3), 237–276.

Fisher, C.M., 1965. The Circle of Willis: anatomical variations. Vasc. Dis. 2, 99–105.

Fouda, A.Y., Fagan, S.C., Ergul, A., 2019. The brain vasculature and cognition: renin-angiotensin system, endothelin and beyond. Arterioscler. Thromb. Vasc. Biol. 39 (4), 593–602.

González Ballester, M.A., Zisserman, A.P., Brady, M., 2002. Estimation of the partial volume effect in MRI. Med. Image Anal. 6 (4), 389–405.

Gorelick, P.B., Furie, K.L., Iadecola, C., Smith, E.E., Waddy, S.P., Lloyd-Jones, D.M., Bae, H.J., Bauman, M.A., Dichgans, M., Duncan, P.W., Girgus, M., Howard, V.J., Lazar, R.M., Seshadri, S., Testai, F.D., van Gaal, S., Yaffe, K., Wasiak, H., Zerna, C., 2017. Defining optimal brain health in adults. A presidential advisory from the American Heart Association/American Stroke Association. Stroke 48 (10), 284–303.

Gutiérrez, J., 2020. Heterogeinity of the circle of Willis and its implication in hippocampal perfusion. Brain 43 (7), e58.

Haast, R.A.M., Kashyap, S., Yousif, M.D., Ivanov, D., Poser, B.A., Khan, A.R., 2021. Delineating perfusion and the effects of vascularisation patterns across the hippocampal subfields at 7T. 29th Annual Meeting of International Society of Magnetic Resonance in Medicine. ISMRM, virtual meeting.

Hartkamp, N.S., et al., 2013. Mapping of cerebral perfusion territories using territorial arterial spin labeling: techniques and clinical application. NMR Biomed. 26 (8), 901–912.

Hashemi, S.M., Mahmoodi, R., Amirjamshidi, A., 2013. Variations in the Anatomy of the Willis' circle: a 3-year cross-sectional study from Iran (2006-2009). Are the distributions of variations of circle of Willis different in different populations? Result of an anatomical study and review of literature. Surg. Neurol. Int. 4, 65.

Henry, B.M., Roy, J., Ramakrishnan, P.K., Vikse, J., Tomaszewski, K.A., Walocha, J.A., 2015. Association of migraine headaches with anatomical variations of the Circle of Willis: evidence from a meta-analysis. Neurol. Neurochir. Pol. 49 (4), 272–277.

Hindenes, L.B., Håberg, A.K., Johnsen, L.H., Mathiesen, E.B., Robben, D., Vangberg, T.R., 2020. Variations in the Circle of Willis in a large population sample using 3D TOF angiography: the Tromsø Study. PLoS One 15 (11), e0241373.

Hoksbergen, A.W., Fülesdi, B., Legemate, D.A., Csiba, L., 2000a. Collateral configuration of the circle of Willis. Transcranial color-coded duplex ultrasonography and comparison with post-mortem anatomy. Stroke 31 (6), 1346–1351.

Hoksbergen, A.W., Legemate, D.A., Ubbink, D.T., Jacobs, M.J., 2000b. Collateral variations in circle of Willis in atherosclerotic population assessed by means of transcranial color-coded duplex ultrasonography. Stroke 31 (7), 1656–1660.

Hoksbergen, A.W., Legemate, D.A., Csiba, L., Csáti, G., Síró, P., Fülesdi, B., 2003. Absent collateral function of the circle of Willis as risk factor for ischemic stroke. Cerebrovasc. Dis. 16 (3), 191–198.

Huck, J., Wanner, Y., Fan, A.P., Jaeger, A.T., Grahl, S., Scheneider, U., Villringer, A., Steele, C.J., Tardif, C.L., Bazin, P.L., Gauthier, C.J., 2019. High resolution atlas of the venous brain vasculature from 7 T quantitative susceptibility maps. Brain Struct. Funct. 224, 2467–2485.

Hyodoh, H., Sato, T., Onodera, M., Washio, H., Hasegawa, T., Hatakenaka, M., 2012. Vascular measurement changes observed using postmortem computed tomography. Jpn. J. Radiol. 30 (10), 840–845.

Jack, C.R., Bennett, D.A., Blennow, K., Carrillo, M.C., Feldman, H.H., Frisoni, G.B., Hampel, H., Jagust, W.J., Johnson, K.A., Knopman, D.S., Petersen, R.C., Scheltens, P., Sperling, R.A., Dubois, B., 2016. A/T/N: an unbiased descriptive classification scheme for Alzheimer disease biomarkers. Neurology 87 (5), 539–547.

Jones, J.D., Castanho, P., Bazira, P., Sanders, K., 2021. Anatomical variations of the circle of Willis and their prevalence, with a focus on the posterior communicating artery: a literature review and meta-analysis. Clin. Anat. 34 (7), 978–990.

Jones, S.E., 2021. Neuroimaging at 3T vs 7T, is it really worth it? Magn. Reson. Imaging Clin. 29 (1), 1–12.

Jongen, J.C., Franke, C.L., Ramos, L.M., Wilmink, J.T., van Gijn, J., 2004. Direction of flow in posterior communicating artery on magnetic resonance angiography in patients with occipital lobe infarcts. Stroke 35 (1), 104–108.

Kapoor, K., Singh, B., Dewan, L.I., 2008. Variations in the configuration of the circle of Willis. Anat. Sci. Int. 83, 96–106.

Karatas, A., Coban, G., Cinar, C., Oran, I., Uz, A., 2015. Assessment of the circle of willis with cranial tomography angiography. Med. Sci. Monit. 21, 2647–2652.

Krabbe-Hartkamp, M.J., van der Grond, J., de Leeuw, F.E., de Groot, J.C., Al-gra, A., Hillen, B., et al., 1998. Circle of Willis: morphologic variation on three-dimensional time-of-flight MR angiograms. Radiology 207, 103–111.

Leeuwis, A.E., Smith, L.A., Melbourne, A., Huhges, A.D., Richards, M., Prins, N.D., Sokolska, M., Atkinson, D., Tillin, T., Jäger, H.R., Chaturvendi, N., van der Flier, W.M., Barkhof, F., 2018. Cerebral blood flow and cognitive functioning in a community-based, multi-ethnic cohort: the SABRE study. Front. Aging Neurosci 10, 279.

Linn, J., Halpin, A., Demaerel, P., Ruhland, J., Giese, A.D., Dichgans, M., van Buchem, M.A., Bruckmann, H., Greenberg, S.M., 2010. Prevalence of superficial siderosis in patients with cerebral amyloid angiopathy. Neurology 74 (17), 1346–1350.

Losordo, D.W., Cooke, J.P., 2016. Functional response to metabolic demand. Stem Cell and Gene Therapy for Cardiovascular Disease. Elsevier doi:10.1016/C2014-0-00701-0.

Lisman, J., Buzsáki, G., Eichenbaum, H., Nadel, L., Ranganath, C., Redish, A.D., 2017. Viewpoints: how the hippocampus contributes to memory, navigation and cognition. Nat. Neurosci. 20 (11), 1434–1447.

Maass, A., Düzel, E., Goerke, M., Becke, A., Sobieray, U., Neumann, K., et al., 2015. Vascular hippocampal plasticity after aerobic exercise in older adults. Mol. Psychiatry 20, 585–593.

Marinković, S., Milisavljević, M., Puskas, L., 1992. Microvascular anatomy of the hippocampal formation. Surg. Neurol. 37 (5), 339–349.

Mattern, H., Sciarra, A., Godenschweger, F., Stucht, D., Lüsebrink, F., Rose, G., Speck, O., 2018. Prospective motion correction enables highest resolution time-of-flight angiography at 7T. Magn. Reson. Med. 80 (1), 248–258.

Mattern, H., Speck, O., 2020. Vessel distance mapping. 36th Annual Scientific Meeting of European Society for Magnetic Resonance in Medicine and Biology. ESMRMB September, Online doi:10.1007/s10334-020-00876-y.

Mattern, H., 2021. Vessel distance mapping of the aging subcortical venous vasculature; 37th Annual Scientific Meeting of European Society for Magnetic Resonance in Medicine and Biology. ESMRMB doi:10.1007/s10334-021- 00947-8, October 2021 Online.

Mattern, H., Schreiber, S., Speck, O., 2021. Vessel distance mapping for deep gray matter structures. 29th Annual Meeting of International Society of Magnetic Resonance in Medicine. ISMRM, May, virtual meeting.

McDonald, A.J., Mott, D.D., 2017. Functional neuroanatomy of amygdalohippocampal interconnections and their role in learning and memory. J. Neurosci. Res. 95 (3), 797–820.

Michaelis, E.K., 2012. selective neuronal vulnerability in the hippocampus: relationship to neurological diseases and mechanisms for differential sensitivity of neurons to stress. In: The Clinical Neurobiology of the Hippocampus, pp. 54–76.

Montine, T.J., Cholerton, B.A., Corrada, M.M., Edland, S.D., Flanagan, M.E., Hemmy, L.S., Kawas, C.H., White, L.R., 2019. Concepts for brain aging: resistance, resilience, reserve, and compensation. Alzheimers Res. Ther. 11 (1), 22.

Nurkiewicz, T.R., Frisbee, J.C., 2010. Boegehold. In: Assessment of Vascular reactivity. *Comprehensive Toxicology*. Elsevier, pp. 133–148.

Oumer, M., Alemayehu, M., Muche, A., 2021. Association between circle of Willis and ischemic stroke: a systematic review and meta-analysis. BMC Neurosci. 22 (1), 3.

Pascalau, R., Padurean, V.A., Bartos, D., Bartos, A., Szabo, B.A., 2019. The geometry of the circle of Willis anatomical variants as a potential cerebrovascular risk factor. Turk. Neurosurg. 29 (2), 151–158.

Peh, W.C.G., 2014. Pitfalls in Diagnostic Radiology. Springer, pp. 212–214.

Perosa, V., Priester, A., Ziegler, G., Cárdenas-Blanco, A., Dobisch, L., Spallazzi, M., Assmann, A., Maass, A., Speck, O., Oltmer, J., Heinze, H.J., Schreiber, S., Düzel, E., 2020. Hippocampal vascular reserve associated with cognitive performance and hippocampal volume. Brain 143 (2), 622–634.

Scheumann, V., Schreiber, F., Perosa, V., Assmann, A., Mawrin, C., Garz, C., Heinze, H.J., Görtler, M., Düzel, E., Vielhaber, S., Charidimou, A., Schreiber, S., 2020. MRI phenotyping of underlying cerebral small vessel disease in mixed hemorrhage patients. J. Neurol. Sci. 419, 117173. doi:10.1016/j.jns.2020.117173.

Schreiber, S., DiFrancesco, J.P., 2020. Impaired occipital cerebrovascular reactivity as a biomarker for vascular β-amyloid. Neurology 95 (10), 415–416.

Shubhangi, Y., 2018. Variations of circle of Willis in human cadavers. Int. J. Anat. Var. 11 (2), 43–45.

Silva Neto, Â.R., Câmara, R.L., Valença, M.M., 2012. Carotid siphon geometry and variants of the circle of Willis in the origin of carotid aneurysms. Arq. Neuropsiquiatr. 70 (12), 917–921.

Shaban, A., Albright, K.C., Boehme, A.K., Martin-Schild, S., 2013. Circle of Willis Variants: fetal PCA. Stroke Res. Treat. 2013, 105937.

Spallazzi, M., Dobisch, L., Becke, A., Caffarra, P., Düzel, E., 2019. Hippocampal vascularization patterns: a high resolution 7T time-of-flight magnetic resonance angiography study. Neuroimage Clin. 39, 561–563.

Stern, Y., Barnes, C.A., Grady, C., Jones, R.N., Raz, N., 2019. Brain reserve, cognitive reserve, compensation, and maintenance: operationalization, validity, and mechanisms of cognitive resilience. Neurobiol. Aging 83, 124–129.

Tatu, L., Vuillier, F., 2014. Structure and vascularization of the human hippocampus. Front. Neurol. Neurosci. 34, 18–25.

Uchimura, J., 1928. Über die Gefäßversorgung des Ammonshornes Zeitschrift für die gesamte. Neurol. Psychiatr 112, 1–19.

Vockert, N., Perosa, V., Ziegler, G., Schreiber, F., Priester, A., Spallazzi, M., Garcia-Garcia, B., Aruci, M., Mattern, H., Haghikia, A., Düzel, E., Schreiber, S., Maass, A., 2021. Hippocampal vascularization patterns exert local and distant effects on brain structure but not vascular pathology in old age. Brain Commun. 3 (3), 1–14 fcab127.

Wardlaw, JM, Brindle, W, Casado, AM, Shuler, K, Henderson, M, Thomas, B, Macfarlane, J, Muñoz Maniega, S, Lymer, K, Morris, Z, Pernet, C, Nailon, W, Ahearn, T, Mumuni, AN, Mugruza, C, McLean, J, Chakirova, G, Tao, YT, Simpson, J, Stanfield, AC, Johnston, H, Parikh, J, Royle, NA, De Wilde, J, Bastin, ME, Weir, N, Farrall, A, Valdes Hernandez, MC, Collaborative Group, SINAPSE, 2012. A systematic review of the utility of 1.5 versus 3 Tesla magnetic resonance brain imaging in clinical practice and research. Eur Radiol 22 (11), 2295–2303 Nov.

Wardlaw, J.M., Smith, E.E., Biessels, G.J., et al., 2013. Neuroimaging standards for research into small vessel disease and its contribution to ageing and neurodegeneration. Lancet Neurol. 12 (8), 822–838.

Westphal, L.P., Lohaus, N., Winklhofer, S., Manzolini, C., Held, U., Steigmiller, K., Hamann, J.M., El Amki, M., Dobrocky, T., Panos, L.D., Kaesmacher, J., Fischer, U., Heldner, M.R., Luft, A.R., Gralla, J., Arnold, M., Wiest, R., Wegener, S., 2021. Circle of Willis variants and their association with outcome in patients with middle cerebral artery-M1-occlusion stroke. Eur. J. Neurol. 28 (11), 3682–3691.

Wiesmann, M., Leeuw, F.E., 2020. Vascular reserve in brain resilience: pipes or perfusion? Brain 143 (2), 390–392.

Xu, W., Bai, Q., Dong, Q., Guo, M., Cui, M., 2022. Blood-brain barrier dysfunction and the potential mechanisms in chronic cerebral hypoperfusion induced cognitive impairment. Front. Cell Neurosci 16, 870674. doi:10.3389/fncel.2022.870674.

Zeidman, P., Maguire, E.A., 2016. Anterior hippocampus the anatomy of perception, imagination and episodic memory. Nat. Rev. Neurosci. 17 (3), 173–182.

Zijlmans, M., Huibers, C.J., Huiskamp, G.J., de Kort, G.A., Alpherts, W.C., Leijten, F.S., Hendrikse, J., 2012. The contribution of posterior circulation to memory function during the intracarotid amobarbital procedure. J. Neurol. 259 (8), 1632–1638.

Zhang, Z., Karasan, E., Gopalan, K., Liu, C., Lustig, M., 2021. DiSpect: displacement spectrum imaging of flow and tissue perfusion using spin-labeling and stimulated echoes. Magn. Reson. Med. 86 (5), 2468–2481.

Zheng, Z., Chopp, M., 2022. Mechanisms of plasticity remodeling and recovery. Stroke doi:10.1016/C2018-0-02267-7.

Zhu, G., Yuan, Q., Yang, J., Yeo, J.H., 2015. Experimental study of hemodynamics in the circle of Willis. Biomed. Eng. 14 (Suppl 1), S10.